Medical Physics
The International Journal of Medical Physics Research and Practice

Total inhomogeneity correction including chemical shifts and susceptibility by view angle tilting

Z. H. Cho, D. J. Kim, and Y. K. Kim

Citation: Medical Physics **15**, 7 (1988); doi: 10.1118/1.596162
View online: http://dx.doi.org/10.1118/1.596162
View Table of Contents: http://scitation.aip.org/content/aapm/journal/medphys/15/1?ver=pdfcov
Published by the American Association of Physicists in Medicine

Articles you may be interested in

Effective Algorithm for Detection and Correction of the Wave Reconstruction Errors Caused by the Tilt of Reference Wave in Phaseshifting Interferometry
AIP Conf. Proc. **1236**, 91 (2010); 10.1063/1.3426174

Wet chemical analysis for the semiconductor industry—a total view
AIP Conf. Proc. **449**, 703 (1998); 10.1063/1.56916

Angle-corrected doppler-shift attenuation analysis
AIP Conf. Proc. **392**, 321 (1997); 10.1063/1.52475

The effect of tilt angle on As implants in Si
J. Vac. Sci. Technol. A **13**, 1321 (1995); 10.1116/1.579558

The extended net fractional depth dose: Correction for inhomogeneities, including effects of electron transport in photon beam dose calculation
Med. Phys. **14**, 84 (1987); 10.1118/1.596107

Total inhomogeneity correction including chemical shifts and susceptibility by view angle tilting

Z. H. Cho,[a] D. J. Kim, and Y. K. Kim
Department of Electrical Sciences, Korea Advanced Institute of Science, P. O. Box 150 Cheongyangni, Seoul, Korea

(Received 25 June 1987; accepted for publication 28 September 1987)

A correction technique of the total magnetic field inhomogeneity effects including the localized object induced inhomogeneities such as chemical shift and susceptibility is developed and its usefulness is experimentally demonstrated. With this new and simple technique all the inhomogeneity induced artifacts can be corrected simultaneously. The basic idea of this method is to add a compensation gradient of the same amplitude as the selection gradient in simultaneity with the reading gradient in such a way that the view angle is tilted. Thereby all the inhomogeneity induced geometrical shifts and hence the intensity changes are corrected, since the addition of the compensation which is independent from the field inhomogeneities including both chemical shifts and susceptibility. This technique has been theoretically examined and its usefulness is demonstrated by experiments.

I. INTRODUCTION

The recent trend of increasing magnetic fields for nuclear magnetic resonance (NMR) imaging has improved the image quality and also delivered potentially available information such as the effects of the chemical shift and magnetic susceptibility.[1–5] This wealth of available information, however, cannot be fully utilized unless proper techniques are employed. In addition, these inhomogeneities often appear as artifacts and the degree of artifact appearance becomes larger proportionally with the increase of the field strength. For conventional proton imaging, therefore, these inhomogeneity effects are the main sources of the artifacts usually observed in high field NMR imaging. Such artifacts include chemical-shift related discrete position shifts and continuous position shifts due to cumulative geometrical field distortions affected by susceptibility in the direction of reading gradient.[6]

A field inhomogeneity then can be generally categorized as (i) a static magnetic field, (ii) a chemical shift, and (iii) susceptibility induced field inhomogeneities. The static field inhomogeneity can usually be corrected by the measurement or mapping of the field prior to imaging[7,8] and often appears as slowly varying field perturbation which would not seriously affect the overall image quality unless the chemical-shift imaging or similar imaging is of interest. Chemical-shift and susceptibility effects are, however, both highly localized and indistinguishable from each other in many cases.[6] In addition to the above, an eddy current due to gradient pulsing generates the time varying inhomogeneity, which also affects the final image similar to the other effects.[9] So far the chemical-shift artifact correction has been studied successfully using a number of techniques such as an echo time encoding, etc.[1,2,4]

The chemical-shift and susceptibility effects or the measurements of such effects are often important and provide valuable information. Artifacts associated with those effects, however, are often very serious and require correction in conventional proton imaging as well as in the imaging of other nuclei. Correction of these artifacts, however, requires rather complex data acquisition schemes or an individual correction method of each artifact, e.g., chemical-shift correction using an echo time encoding technique and susceptibility correction by other schemes such as the postprocessing, etc.

In this paper, we have described a method by which all the inhomogeneity dependent artifacts such as the artifacts resulting from the chemical shift, susceptibility, and static field inhomogeneity, can all be simultaneously eliminated. An additional advantage of this technique is that the correction scheme is very simple. It requires only one set of imaging sequences which are a minor modification of the conventional two-dimensional (2-D) Fourier imaging sequence (see Fig. 1).

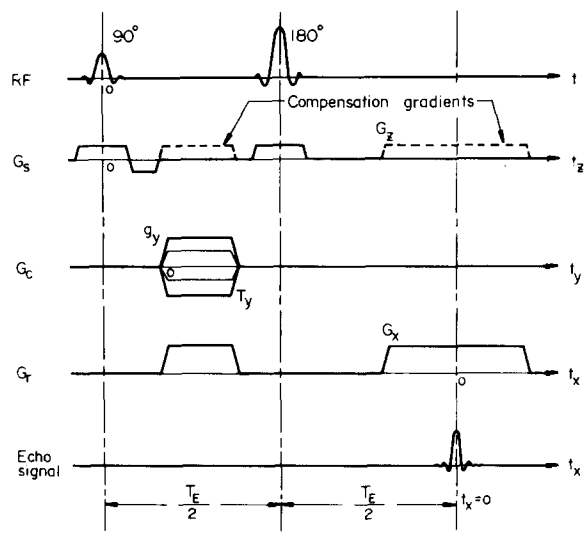

FIG. 1. Pulse sequence for the generalized inhomogeneity correction scheme proposed in this paper. This sequence is based on the conventional spin-echo sequence (solid line) with an addition of the compensation gradient G_z as shown (broken line). Strength of the compensation gradient should be identical to the selection gradient and be applied simultaneously with the reading gradient (G_x in this case). Tilted view angle then appears as $\theta = \tan^{-1}(G_z/G_x)$.

 0094-2405/88/010007-05$01.20 © 1988 Am. Assoc. Phys. Med.

Generally, field inhomogeneity effects on the image are geometrical distortion and intensity change due to geometrical shifts. For example, in a transaxial imaging, field nonuniformity in the direction of the slice selection (z), i.e., axial nonuniformity within a slice, is relatively small compared with transversal plane (x,y) nonuniformity. In this case, the x or y direction becomes the reading gradient direction and therefore the geometrical shifts appear in the x or y direction. In the proposed scheme, correction is achieved by the addition of a compensation gradient of the same amplitude as the selection gradient in the selection direction so that the view angle is tilted slightly. This compensation gradient is applied in simultaneity with the reading gradient so that the appropriate tilting angle ($\theta = \tan^{-1} G_z/G_x$) is formed (see Fig. 1). The proposed scheme is easy to implement and results in overall inhomogeneity correction by a simple measurement sequence.

Basic theory, computer simulated results, and experimentally obtained images with the proposed technique are presented, and future potential applications are discussed.

II. EFFECTS OF FIELD INHOMOGENEITY AND GENERALIZED CORRECTION METHOD

As discussed, there are mainly three different types of field inhomogeneity, namely, static field inhomogeneity, chemical shift, and susceptibility induced field inhomogeneity, respectively. Assuming that the total sum of these inhomogeneity or spatially varying function is $h(x,y,z)$ or simply $h(x,y)$ for a given slice, a Fourier imaging equation then can be written as (see solid line in Fig. 1)

$$S(t_x,g_y) = \int_y\int_x\int_{z_1}^{z_2} \rho(x,y,z)\exp[-i\gamma h(x,y)t_x]\exp[-i\gamma(xG_xt_x + yg_yT_y)]\,dz\,dx\,dy$$

$$\text{or} \quad = \int_y\int_x\int_{-(L_s/2)+L_c(x,y)}^{(L_s/2)+L_c(x,y)} \rho(x,y,z)\exp\left\{-i\gamma\left[\left(x + \frac{h(x,y)}{G_x}\right)G_xt_x + yg_yT_y\right]\right\} dz\,dx\,dy, \tag{1}$$

where, γ is gyromagnetic ratio, $\rho(x,y,z)$ is the spin density function, G_x and g_y are reading and coding gradient strengths, L_s is the the slice thickness determined by the radiofrequency (rf) bandwidth F_B and the selection gradient field strength G_s, L_c is the position variation due to the inhomogeneity, and z_1 and z_2 are the lower and upper limits of the region selected by selective rf pulse, respectively, i.e.,

$$L_s = 2\pi F_B/\gamma G_s \text{ cm}, \quad L_c(x,y) = -h(x,y)/G_s \text{ cm},$$
$$z_1 = -(L_s/2) + L_c(x,y), \text{ and } z_2 = (L_s/2) + L_c(x,y). \tag{2}$$

As discussed above, if we apply a compensation gradient along the selection gradient of the same magnitude (in amplitude) as the selection gradient in simultaneity with the reading gradient (see broken line in Fig. 1), Eq. (1) is written as

$$S(t_x,g_y) = \int_y\int_x\int_{-(L_s/2)+L_c(x,y)}^{(L_s/2)+L_c(x,y)} \rho(x,y,z) \times\exp(-i\gamma zG_zt_z) \times\exp[-i\gamma\{\{x + [h(x,y)/G_x]\}G_xt_x + yg_yT_y)]\,dz\,dx\,dy. \tag{3}$$

By change of variable $z = z^* - h(x,y)/G_s$ and by assuming that $t_z = t_x$ and $G_z = G_s$, Eq. (3) becomes

$$S(t_x,g_y) = \int_y\int_x\int_{z_1^*}^{z_2^*} \rho\left(x,y,z^* - \frac{h(x,y)}{G_s}\right) \times\exp(-i\gamma\{z^* - [h(x,y)/G_s]\}G_st_x) \times\exp[-i\gamma\{\{x + [h(x,y)/G_x]\}G_xt_x + yg_yT_y)]|J|\,dz^*\,dx\,dy, \tag{4}$$

where z_1^* and z_2^* are $-L_s/2$ and $L_s/2$, respectively, and J is the Jacobian which is an unity in this case, i.e.,

$$J(x,y) = \frac{\partial z}{\partial z^*} = 1\Big/\frac{\partial z^*}{\partial z} = 1. \tag{5}$$

Equation (4) can be further simplified by elimination of the inhomogeneity terms related to t_x, i.e.,

$$S(t_x,g_y) = \int_y\int_x\int_{-L_s/2}^{L_s/2} \rho\left(x,y,z^* - \frac{h(x,y)}{G_s}\right) \times\exp(-i\gamma z^*G_st_x) \times\exp[-i\gamma(xG_xt_x + yg_yT_y)]\,dz^*\,dx\,dy. \tag{6}$$

For simplicity of formulation, let us assume that the spin density function $\rho(x,y,z)$ is constant with respect to the z direction within the selected slice whose thickness is L_s. With this assumption, the spin density function $\rho[x,y,z^* - h(x,y)/G_s]$ of Eq. (6) can be replaced with $\rho[x,y,z_o^* - h(x,y)/G_s]$, where z_o^* is a constant value of z^*. Thus Eq. (6) is written as

$$S(t_x,g_y) = \int_{-L_s/2}^{L_s/2} \exp(-i\gamma z^*G_st_x)dz^* \int_y\int_x \rho\left(x,y,z_o^* - \frac{h(x,y)}{G_s}\right)\exp[-i\gamma(xG_xt_x + yg_yT_y)]\,dx\,dy$$

$$\text{or} \quad = \left[L_s\,\text{sinc}\left(\gamma G_s\frac{L_s}{2}t_x\right)\right] \int_y\int_x \rho\left(x,y,z_o^* - \frac{h(x,y)}{G_s}\right)\exp[-i\gamma(xG_xt_x + yg_yT_y)]\,dx\,dy. \tag{7}$$

In Fig. 2, the relation of z and z^* in connection with an inhomogeneity function $h(x,y)$ is illustrated. The image function $\tilde{\rho}(x,y)$ can be obtained by 2-D Fourier transform of Eq. (7), i.e.,

$$\tilde{\rho}(x,y) = \int_y\int_x S(t_x,g_y)\exp[i(w_x x + w_y y)]dw_x\, dw_y$$

$$= \left\{\int_y\int_x \left[L_s \operatorname{sinc}\left(\gamma G_s \frac{L_s}{2} t_x\right)\right] \exp[i(w_x x + w_y y)]dw_x\, dw_y\right\} \circledast \left[\rho\left(x,y,z_o^* - \frac{h(x,y)}{G_s}\right)\right]$$

or

$$= \frac{2}{\gamma G_s} \Pi\left[x \Big/ \left(\frac{2\pi F_B}{\gamma G_x}\right)\right] \circledast \rho\left(x,y,z_o^* - \frac{h(x,y)}{G_s}\right), \tag{8}$$

where $\circledast$ is the linear convolution operator and Π is a rectangular function defined by

$$\Pi(x) = \begin{cases} 1, & -1/2 \leqslant x \leqslant 1/2, \\ 0, & \text{otherwise}. \end{cases} \tag{9}$$

Equation (8) shows, therefore, that the image function $\rho[x,y,z_o^* - h(x,y)/G_s]$ is now convolved (blurred) with a rectangular function $\Pi[x/(2\pi F_B/\gamma G_x)]$. In practice, however, $\Pi[\cdot]$ is made relatively narrow and therefore effects on image blurring are usually negligible, i.e.,

$$\tilde{\rho}(x,y) \cong \rho\{x,y,z_o^* - [h(x,y)/G_s]\}. \tag{10}$$

By applying a compensation gradient in simultaneity with the reading gradient, the view angle is tilted by $\theta = \tan^{-1}(G_z/G_x)$. Therefore, the view angle will decrease by increase of G_x or by decrease of G_z. It should also be mentioned that the optimal condition $G_z = G_s$ is independent of inhomogeneity term $h(x,y)$, so that the total inhomogeneity artifacts including chemical shift and susceptibility are simultaneously corrected.

In Fig. 3, step by step illustrations of the chemical-shift correction process are given. First, the chemical shift in the z direction is shown in (a), and then the combined shifts in

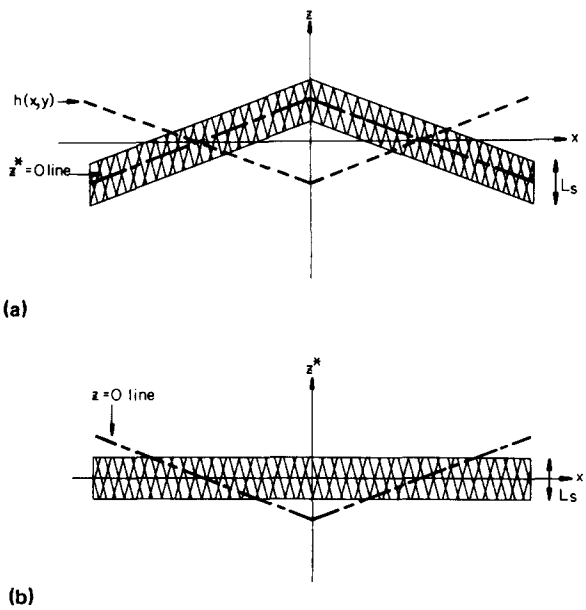

FIG. 2. A simplified inhomogeneity effect is added to illustrate the relation of the z directional coordinate transformation. For simplicity, symmetric and linear one directional (x) inhomogeneity term is considered. (a) shows the inhomogeneity affected slice formation along the z direction while (b) shows the inhomogeneity corrected (straightened) slice formation with coordinate transformation.

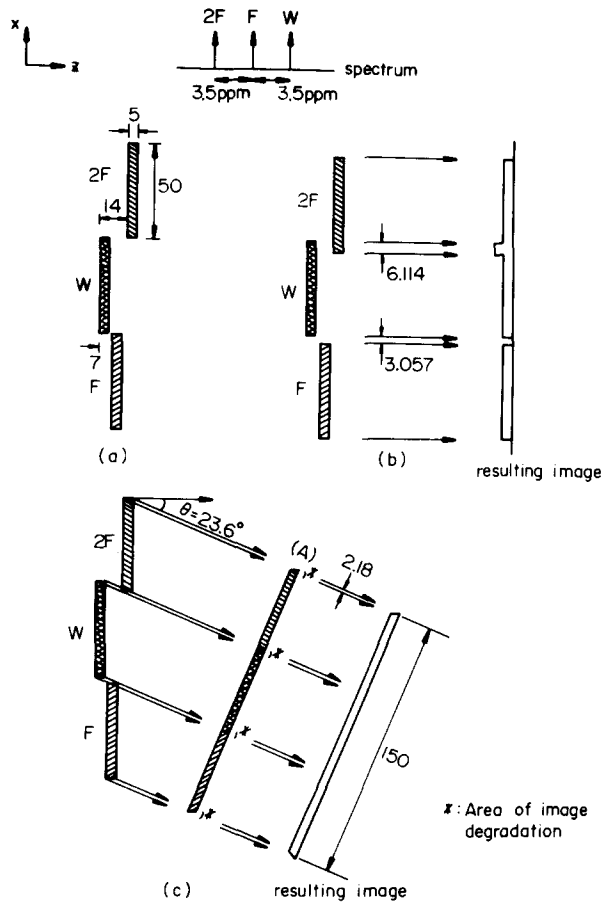

FIG. 3. A simplified step by step view of the generalized inhomogeneity correction method proposed in this paper. For simplicity, three chemical shift peaks are assumed, i.e., water (W), fat (F) which is separated from water by 3.5 ppm, and the other denoted by $2F$ which symbolizes the double chemical shift of 3.5 ppm from water peak. (a) shows the chemical shift in z direction only, (b) shows simultaneous chemical shifts in both x and z directions. Finally, (c) shows the result of the two combined shifts and image seen by tilted view angle θ which results in a corrected image. The small practically negligible image blur which can be seen at the image boundaries is also indicated. This blurring as a result of finite slice thickness is usually so small that it can hardly be observable in normal imaging.

both the selection (z) and reading (x) gradient directions are illustrated in (b). Finally, (c) represents the eventual tilting of the view, thereby eliminating the inhomogeneity effects. Here, $\tilde{\rho}(x,y)$ then represents the inhomogeneity corrected image with small blurring due to the view angle tilting as illustrated in (c).

III. EXPERIMENTAL RESULTS AND DISCUSSIONS

For the demonstration of the correction ability of the proposed method for the chemical-shift and susceptibility dependent geometrical distortions, we have devised a phantom with which elimination of both the chemical-shift and susceptibility effects can be demonstrated. Figure 4(a) shows a simple "water–fat" phantom constructed for the demonstration of chemical shift. Figures 4(b) and 4(c) are the experimentally obtained images of the test phantom shown in (a). As seen from Fig. 4(b), the clear sign of chemical shift is seen in two ways; one is the overlap of the fat and water bases, i.e., the fat is shifted downward thereby overlapped in horizontal boundary line, the other is the shift of two fat columns (circles). In Fig. 4(c), the chemical-shift corrected image using the new tilted view angle technique is shown. Note here the disappearance of both overlapped horizontal lines and the shift of the two fat columns. All the images shown, vertical direction is the direction of reading gradient and the field of view is 256 mm. All the experiments were carried out by the KAIS 2.0 T whole-body superconducting NMR system.

In Fig. 5, a more elaborate phantom is shown by which both the chemical-shift and susceptibility (air–water boundary) dependent geometrical shift effects can be measured. This phantom consisted of a column of distilled water which has relatively long T_1 value compared with conventional water, three columns of 0.02 or 0.01 mM $CuSO_4$ solution which have short T_1's, two columns of air which represent the negative susceptibility compared to the background, two soybean oil columns for fat substitute, and an acryl (which does not generate a signal).

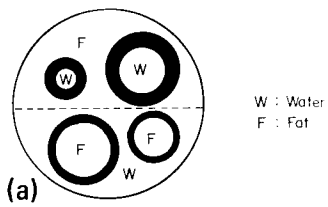

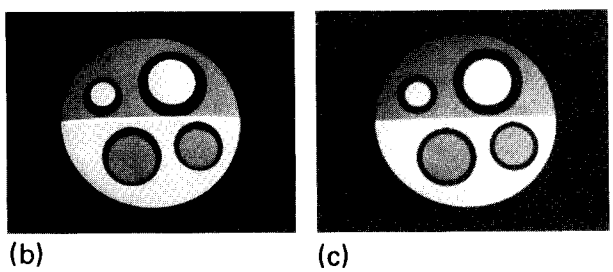

FIG. 4. Experimental imaging results of a phantom which consists of fat and water by KAIS 2.0 T NMR imager. Here (a) is the phantom, (b) and (c) are the images obtained by conventional spin-echo sequence and view angle tilted correction technique, respectively. As seen from (c), a perfectly corrected image is seen. Repetition (T_R) and echo (T_E) times employed are 500 and 30 ms, respectively.

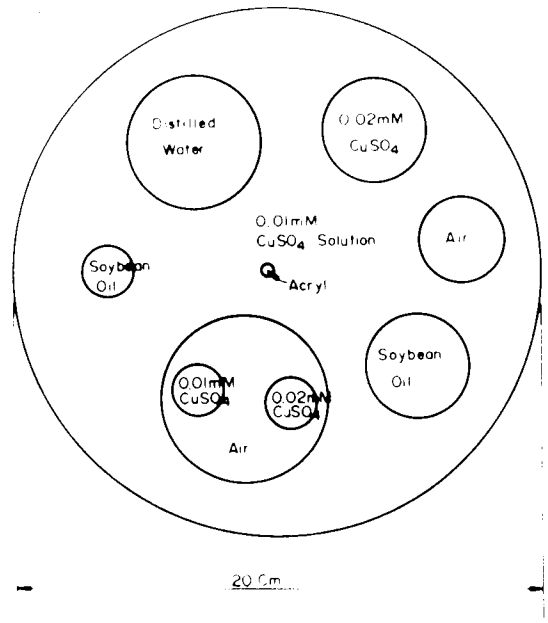

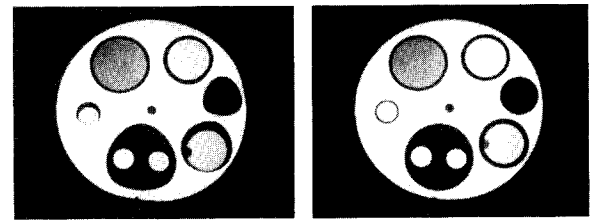

FIG. 5. Experimental imaging results of a more complex phantom which consists of water, fat (soybean oil), and air to demonstrate the chemical shift as well as the susceptibility effect. Here (a) is the phantom, (b) and (c) are the images obtained by using the pulse sequence shown in Fig. 1. The used gradient strength for the compensation gradient was 0.1 G/cm with the x directional reading gradient strength of 0.458 G/cm which eventually would result in a tilting angle of 12.3°.

In Figs. 5(b) and 5(c), experimentally obtained images of the phantom are shown. Figure 5(b) is an image obtained using a normal spin-echo sequence. In this sequence, $T_R = 500$ ms and $T_E = 30$ ms were used. In this image [Fig. 5(b)], clear chemical-shift effects are visible, i.e., two fat columns (circles) are shifted downward while the other water columns (circles) remained still. The two air circles are now clearly distorted by the susceptibility effect. In Fig. 5(c), the corrected image of the same phantom using the proposed view tilting technique is shown. This image, indeed, shows the perfectly corrected image of the complex phantom which contains both the chemical shift and susceptibility as well as the other field inhomogeneity effects. The compensation gradient and reading gradient employed and the subsequent view tilted angle are 0.1 G/cm, 0.458 G/cm, and 12.3°, respectively, with the same T_R and T_E as given in Fig. 5(b).

In Fig. 6, an experimental result of human legs *in vivo* proton imaging is shown. The chemical-shift artifact shown in Fig. 6(a) is obtained by conventional Fourier imaging.

(a)

(b)

FIG. 6. Human *in vivo* experiments of legs. (a) is the uncorrected conventional image. Note that the fat (bone marrow) are shifted downward. (b) is the corrected image of the same legs. In these experiments, $T_R = 1000$ ms and $T_E = 30$ ms are used.

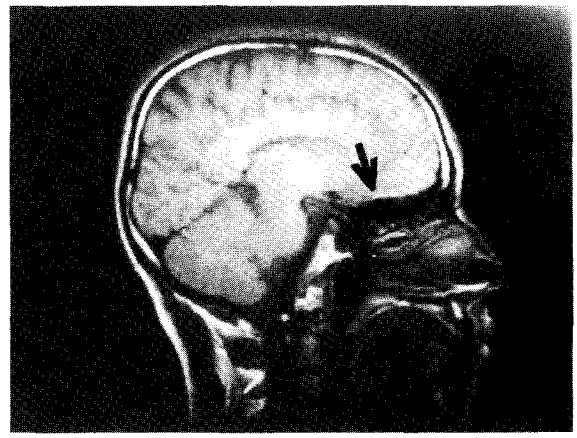

(a)

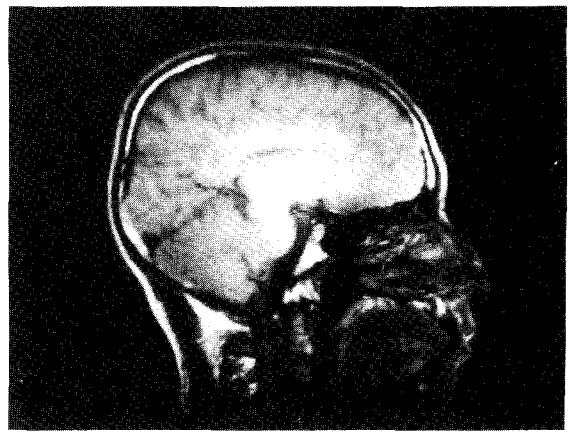

(b)

FIG. 7. *In vivo* experiments of sagittal view human head. (a) and (b) are the uncorrected conventional spin-echo image and corrected image, respectively. $T_R = 300$ ms and $T_E = 30$ ms are used for the experiments. Susceptibility affected artifacts are shown by the arrow in (a).

Figure 6(b) is the corrected image of Fig. 6(a) using the tilted view angle technique proposed in this paper. A remarkably clear fat–water image is obtained by a single sequence of measurement unlike other chemical-shift imaging techniques such as Dixon's method (CHESS technique) or the echo time encoding technique described previously.

Figure 7 demonstrates the susceptibility affected artifacts in human head images and correction of those artifacts by use of view angle tilting. Figure 7(a) is the conventional spin-echo imaging of the human head sagittal view where the relatively dense area shown by the arrow indicates the geometrical shift artifact due to the susceptibility. Figure 7(b) shows the same image corrected by the proposed view angle tilting technique. Note also that the chemical-shift artifact shown in Fig. 7(a) at the top of the head (skin) has also been corrected.

In summary, we found a simple and generalized field inhomogeneity correction technique with which both the chemical shift and the susceptibility and also other field inhomogeneities can be corrected simultaneously by a single sequence. This technique utilizes an additional selection gradient G_z of the same magnitude as the selection gradient in simultaneity with the reading gradient, thereby producing a tilted viewing angle which in turn automatically corrects the field inhomogeneity dependent geometrical shifts.

[a] Present address: Department of Radiological Sciences, University of California, Irvine, CA 92717.

[1] W. T. Dixon, "Simple proton spectroscopic imaging," Radiology **153**, 189 (1984).
[2] Z. H. Cho, O. Nalcioglu, H. W. Park, J. B. Ra, and S. K. Hilal, "Chemical-shift artifact correction scheme using echo-time encoding technique," Magn. Reson. Med. **2**, 253 (1985).
[3] K. Sekihara, M. Kuroda, and H. Kohno, "Image restoration from non-uniform magnetic field influence for direct Fourier NMR imaging," Phys. Med. Biol. **29**, 15 (1984).
[4] E. Feig, F. Greenhleaf, and M. Perlin, "Magnetic resonance imaging with non-uniform fields," Phys. Med. Biol. **31**, 1091 (1986).
[5] M. O'Donnell and W. A. Edelstein, "NMR imaging in the presence of magnetic field inhomogeneities and gradient field nonlinearities," Med. Phys. **12**, 20 (1985).
[6] H. W. Park, Y. M. Ro, and Z. H. Cho, "Measurement of magnetic susceptibility effect in the high field NMR imaging," Phys. Med. Biol. (in press) 1987; K. M. Lüdeke, P. Röschmann, and R. Tischler, "Susceptibility artefacts in NMR imaging," Magn. Reson. Imag. **3**, 329 (1985).
[7] Ching-Ming Lai, "Reconstructing NMR images from projections under inhomogeneous magnetic field and non-linear field gradients," Phys. Med. Biol. **28**, 925 (1983).
[8] A. A. Maudsley, S. K. Hilal, W. H. Perman, and H. E. Simon, "Spatially resolved high resolution spectroscopy by four-dimensional NMR," J. Magn. Reson. **51**, 147 (1983).
[9] Y. S. Kim and Z. H. Cho, "Eddy current compensated field inhomogeneity mapping in NMR imaging," J. Magn. Reson. (in press).